Materials Science & Engineering A 606 (2014) 409–416

Contents lists available at ScienceDirect

Materials Science & Engineering A

journal homepage: www.elsevier.com/locate/msea

Identification of the hardening law of materials with spherical indentation using the average representative strain for several penetration depths

Charbel Moussa [a,*], Xavier Hernot [a,b], Olivier Bartier [a,b], Guillaume Delattre [c], Gérard Mauvoisin [a,b]

[a] LGCGM EA3913, Université de Rennes1-INSA de Rennes, 20 Avenue des Buttes de Coësmes, 35708 Rennes Cedex 7, France
[b] IUT de Rennes 1, 3 rue du Clos Courtel, 35704 Rennes Cedex, France
[c] Faurecia Automotive Seating, Le Pont de Vère, 61100 Caligny, France

ARTICLE INFO

Article history:
Received 27 December 2013
Accepted 26 March 2014
Available online 3 April 2014

Keywords:
Steel alloy
Spherical indentation
Hardening law
Average representative strain
Confidence domain

ABSTRACT

The identification of plastic properties with spherical indentation has been the subject of many studies in the last decades. In the present work, a new method for the determination of the hardening law of materials using the load–displacement curve of a spherical indentation test is proposed. This method is based on the use of an average representative strain. The advantage of the proposed average representative strain is that it is strictly obtained from the material in response to the indentation test. By using various values of penetration depth, the proposed method gives the range of strain for which the hardening law is precisely identified and allows determining a confidence domain that takes into account experimental imprecision and material heterogeneity. The influence of penetration depth and the error formula on the identified Hollomon hardening law are discussed in the present study. The present study clarifies many problems that were observed in previous studies such as the uniqueness of solution and the sensitivity of the indentation test to the plastic parameters of the Hollomon hardening law.

1. Introduction

Knowledge of the hardening law is fundamental in design and formation of metal products. This mechanical property is commonly obtained from tensile test. For cases such as plastically and functionally graded materials, biomedical materials, welded components and thin films, the tensile test cannot be applied. The instrumented indentation test is an excellent substitute in such cases for the standard tensile test [1–9]. Identification of plastic hardening parameters from a load–penetration depth spherical indentation curve (F–h curve) is mostly used and the methods based on the representative strain and stress approach are widely proposed [10–20].

Several methods consist to directly correlate the representative stress and strain to the stress–strain point in the uniaxial tensile test [10,13–15]. Other methods consist to determine the parameters of the Hollomon hardening law from a closed-form expression of the F–h curve as a function of material properties [11,12,16–18,20,21]. For the second group of methods, the full stress–strain response is commonly estimated from the following piecewise power law assumption:

$$\begin{cases} \sigma = E\varepsilon & \text{if} \quad \sigma \le \sigma_y \\ \sigma = E^n \sigma_y^{(1-n)} \varepsilon^n & \text{if} \quad \sigma \ge \sigma_y \end{cases} \tag{1}$$

where σ_y is the yield stress, n is the work hardening exponent and E is Young's modulus.

While the framework for determining the hardening law of materials by considering the F–h curve has been demonstrated to work well for metals, issues of uniqueness [17,22,23] and sensitivity [23–25] have also been identified. Moreover, none of the studies concerning the mechanical characterization using the F–h curve [11,12,16–18,20,21] gave a clear answer on the range of strain for which the hardening law is precisely identified. In some studies, no physical justification was given to explain the reason why the proposed strain can be considered as a representative of spherical indentation [10,16]. In other studies, the use of the representative strain serves as a mathematical trick having no physical basis [11,12,18,20,21].

* Corresponding author. Tel.: +33 2 2323 20 31.
E-mail address: charbel.moussa@univ-rennes1.fr (C. Moussa).

http://dx.doi.org/10.1016/j.msea.2014.03.123
0921-5093/

In a recent study [26], an investigation of the domain in which the solution exists while identifying the hardening law of a material with spherical indentation using the F–h curve was performed. A definition of an average representative strain only based on the material response to the indentation test, i.e. the F–h curve, was also proposed in this study. Based on the use of this average representative strain, a new identification method that allows identifying the hardening law of materials for a well-known range of strain is proposed in the present study. Also, the influence of the penetration depth and the choice of the error formula used in the identification process is investigated and overtaken in the proposed method.

2. Material presentation and experimental results

The studied material denoted 20MnB5 steel (European Standard EN 10083-3, Steelgrade no. 1.5530) is a commercial hot-rolled boron-alloyed case-hardening and heat-treatable steel, provided by Hoesch Hohenlimburg GmbH. The chemical composition in weight is 0.191% C, 1.14% Mn, 0.362% Si, 0.0158% P, 0.0008% S, 0.25% Cr, 0.0014% B, 0.039% Al, 0.027% Ti, 0.017% Mo, 0.025% Cu and 0.06% Ni. The steel has been hot rolled to a thickness of 4.5 mm. All investigations have been performed on the material in the as received condition.

The micrograph in Fig. 1 shows, as a result of the hot rolling, a fine and homogeneous distribution of spheroidized carbides in a ferritic matrix. This microstructure gives excellent properties in the as rolled condition for cold forming, slitting and machining without additional annealing processes. For our study, this type of steel was selected because of this fine, homogeneous microstructure, which leads to a good reproducibility of the indentation tests.

The tensile test and indentation specimens were carefully sectioned with a Precision Cut-Off Machine from the hot rolled sheet. The Vickers hardness (10 Kgf) measurements gave $HV_{10}=155$ for the surface and $HV_{10}=160$ for the core. The true tensile curves obtained for 20MnB5 steel before necking are represented in Fig. 2. The experimental conditions and measurement method for the tensile test were presented in a previous study [6]. Fig. 2 shows that the studied material exhibits a yield stress of about 340 MPa and a non-negligible work hardening. This figure also shows that the Hollomon equation does not describe the entire flow curve for the 20MnB5 steels

The spherical indentation tests were carried out with a tungsten carbide ball of radius 0.5 mm. The indentation bench and the experimental conditions used for the indentation tests were detailed in a previous study [6]. Four spherical indentation curves were obtained from the material. Fig. 3 shows that a satisfying reproducibility of the indentation tests was obtained.

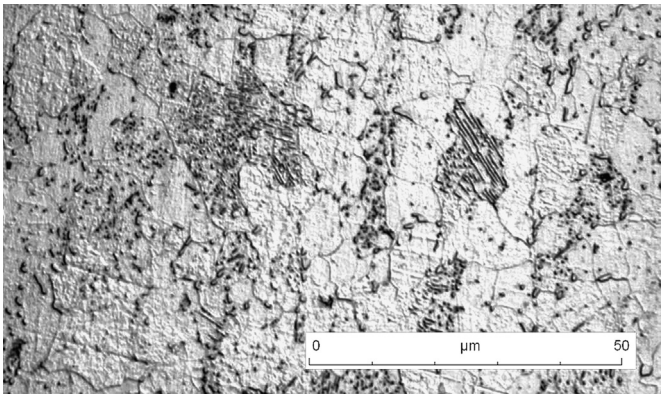

Fig. 1. Microstructure of the 20MnB5 steel alloy.

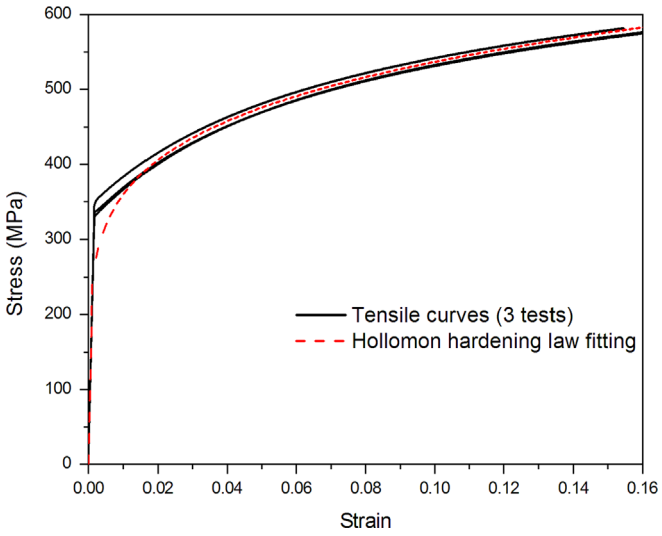

Fig. 2. Uniaxial tensile test curves for 20MnB5 steel alloy [26].

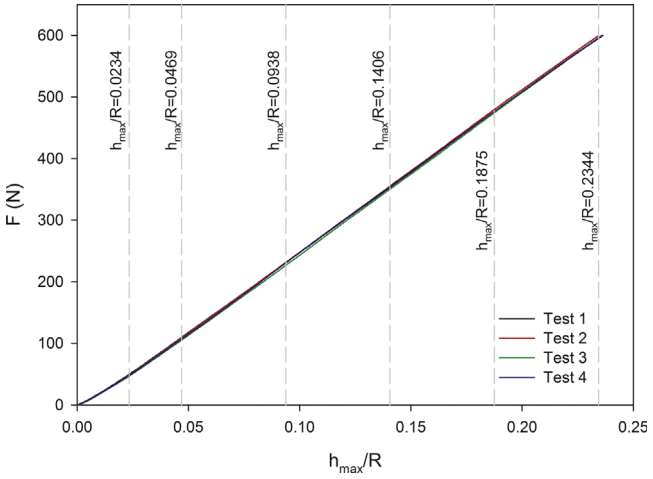

Fig. 3. Spherical indentation curves for 20MnB5 steel alloy.

3. Evaluation of the tensile properties from one value of h_{max}/R ratio

Using the four experimental indentation curves (see Fig. 3), the average curve is determined (average load for every penetration depth). In the present study, only the average curve is used to characterize the material. In order to quantify the gap between two indentation curves, the root mean square error, the following equation, was used

$$E_{RMS}(h_{max}/R)=\sqrt{\frac{1}{h_{max}}\int_0^{h_{max}}(F_1-F_2)^2dh} \quad (2)$$

where R is the spherical indenter radius (0.5 mm), h is the penetration depth, h_{max} is the maximal penetration depth and F_1 and F_2 are the load for the two considered curves. In this section one penetration depth is treated ($h_{max}/R=0.2344$). The characterization procedure consists of calculating the gap, using E_{RMS} (Eq. (2)), between an experimental F–h curve and a number of F–h curves obtained from Finite Element simulations for different Hollomon hardening law parameters. The finite elements (FE) model was presented in a previous study [26]. The elastic properties of the simulated materials

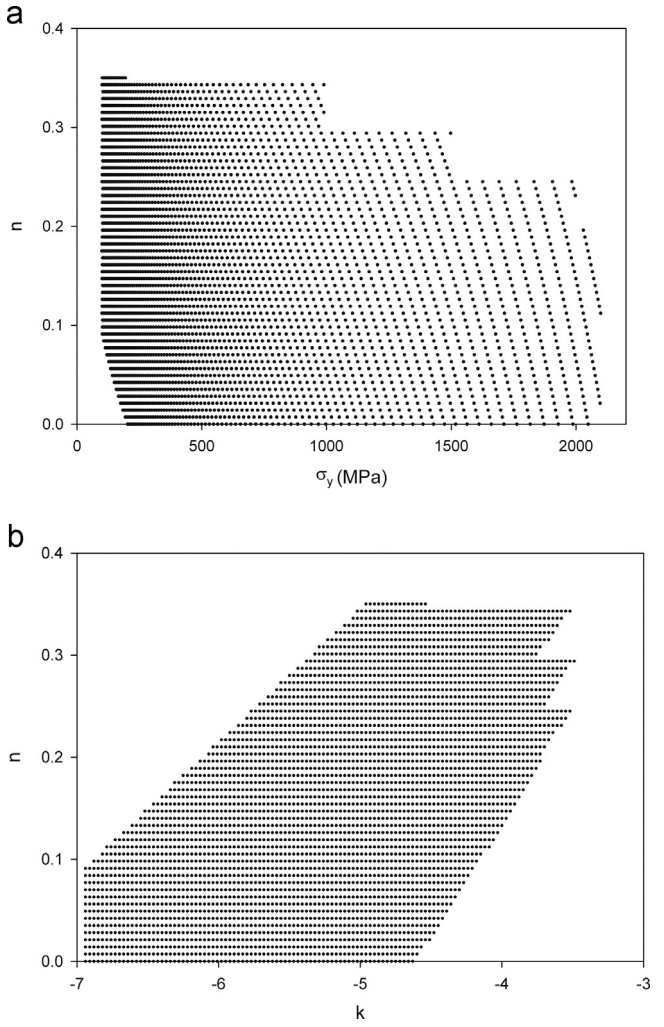

Fig. 4. (a) Materials plastic properties used for the database in [σ_y, n], and (b) [k, n] diagrams.

correspond to the elastic properties of the steels, i.e. $E=210$ GPa and $\nu=0.3$. A database was built up from F–h curves obtained from finite element simulations of the spherical indentation test with different combinations of plastic properties presented in Fig. 4a.

The E_{RMS} distribution in [σ_y, n] diagram is presented in Fig. 5. As presented in the previous study [26], the E_{RMS} distribution takes a particular form of a cone with an elliptical base in the [k, n] diagram, where k is defined as follow:

$$k=(1-n)\ln\left(\frac{\sigma_y}{E}\right) \tag{3}$$

Since the E_{RMS} distribution form (cone with an elliptical base) is known in [k, n] diagram, the values of the hardening law parameter sets of the database were chosen to be regular in [k, n] diagram (Fig. 4b).

The mathematical equation of this cone, used to determine the Hollomon hardening law of the material, is

$$E_{ellipse}=\sqrt{\left(\frac{x}{X}\right)^2+\left(\frac{y}{Y}\right)^2} \tag{4}$$

with

$$x=(k-k_0)\cos\ \theta_{aR}+(n-n_0)\sin\ \theta_{aR} \tag{5}$$

and

$$y=-(k-k_0)\sin\ \theta_{aR}+(n-n_0)\cos\ \theta_{aR} \tag{6}$$

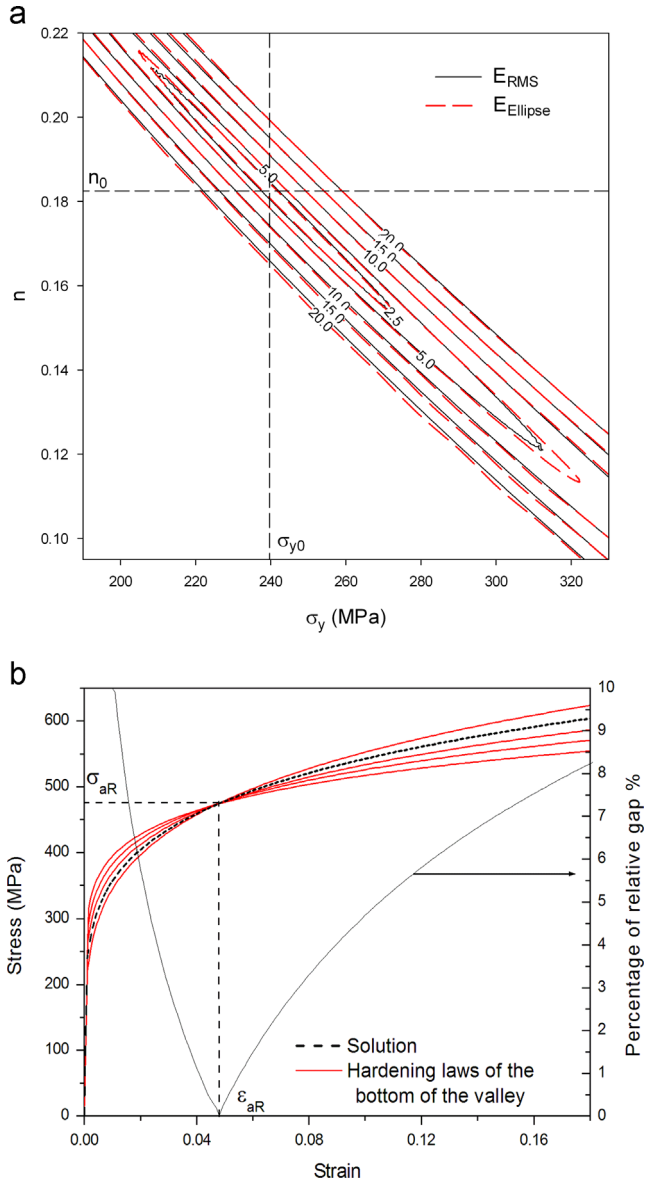

Fig. 5. (a) Comparison between the ERMS distributions obtained from the database and the cone with the elliptical base [26]. (b) Hardening law of the materials for which the material parameter sets (σ_y, n) are located in the bottom of the valley (see Fig. 5(a)) and percentage of the maximal relative gap between these curves [26].

where X and Y are the parameters that indicates the dimensions of the elliptical base for one specific value of error. The dimensional unit of X and Y is the inverse of the dimensional unit of $E_{ellipse}$. K_0 and n_0 are the coordinates of the summit of the cone, i.e. the identified solution and θ_{aR} indicates the direction of the principal axis of the ellipse in [k, n] diagram.

The units of $E_{ellipse}$ and E_{RMS} are identical (Newton, in our case).

The comparison between E_{RMS}, obtained from the database, and $E_{ellipse}$ obtained from Eq. (4) is presented in Fig. 5a. In Fig. 5a, it is clearly shown that the $E_{ellipse}$ distribution given by Eq. (4) superimposes perfectly onto the E_{RMS} distribution. This result proves that the considered assumption on the cone with the elliptical base form is correct.

From Fig. 5a, we can notice the presence of a "valley" in the [σ_y, n] diagram in which the E_{RMS} variation is very small. All the (σ_y, n) parameters that are located in the bottom of this valley lead to hardening laws that intersect at one specific strain (Fig. 5b). This strain, which depends on the direction of the valley, was defined

as the average representative strain, ε_{aR} [26]. All the (σ_y, n) parameters which are located at the bottom of the valley lead to F–h curves close to the F–h curve corresponding to the solution. Hence, the F–h curve is mostly influenced by the part of the hardening law which is located around the average representative strain, ε_{aR}. When a material is characterized using the F–h curve, it is this part of the Hollomon hardening law that is mostly characterized and better identified. To determine ε_{aR} the following equation is used [26]:

$$\varepsilon_{ar} = \exp\left(\frac{-1}{\tan\ \theta_{ar}}\right) \tag{7}$$

The 5 parameters, X, Y, n_0, σ_{y0} and θ_{aR}, are obtained from the minimal value of the following cost function:

$$E = \sum (E^i_{RMS} - E^i_{ellipse})^2 \text{ with } E^i_{RMS} - E^i_{ellipse} = 0 \quad \text{if} \quad E^i_{RMS} \geq E_{critical} \tag{8}$$

where i corresponds to each case of the material parameter sets (σ_y, n) that were chosen for the database. It should be noticed that the elliptical cone form was assumed to be in the form of the E_{RMS} distribution near the solution, i.e. where the valley exists. For this reason, $E_{critical}$ was defined in order to use only the material parameter sets that are near the solution to correctly determine the five parameters of the elliptical cone. In this study $E_{critical}$=30 N was chosen for h_{max}/R=0.2344. In the case of h_{max}/R=0.2344, the parameters of the identified hardening law, presented in Fig. 6, are σ_y=240 MPa and n=0.182. The comparison between the identified hardening law and the tensile test curves shows that the identified parameters of the hardening law give a stress–strain curve very close to the experimental tensile test curves.

Furthermore, the proposed identification method [26]allows identifying a confidence domain. When multiple experimental indentation curves are used, differences between these curves are always observed. One cannot obtain two experimental curves that superimpose perfectly because of the experimental imprecision and the material heterogeneity.

In order to quantify those differences, E_{RMS} is calculated between the average experimental F–h curve and each one of the four experimental curves for a h_{max}/R=0.2344.

The values of E_{RMS} obtained between the average curve and the four experimental curves are presented in Table 1. Using the equation of the cone with the elliptical base (Eq. (4)), the ellipse which corresponds to the maximum value of E_{RMS} given in Table 1 is determined. This ellipse (isovalue of E_{RMS}) is presented in [σ_y, n] and [K, n] diagrams (Fig. 7a). All the Hollomon hardening laws parameters that are located inside this ellipse can be considered as solutions. We define the confidence domain (in stress–strain diagram) as the envelope of these hardening laws [26]. The confidence domain, that delimits the hardening laws identified as solutions, is presented in Fig. 7b.

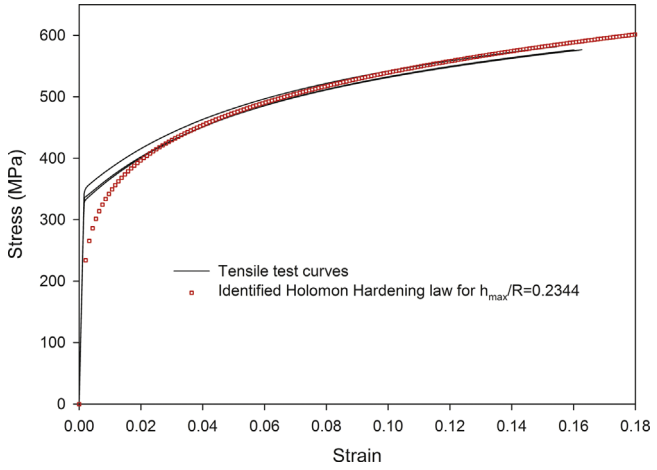

Fig. 6. Comparison between the tensile test curves and the identified hardening law with the elliptical cone definition.

Table 1
Values of root mean square error (E_{RMS}) between the average curve and the four experimental curves.

E_{RMS} (N)					
h_{max}/R	Test 1	Test 2	Test 3	Test 4	Maximum
0.2344	1.17	1.97	2.50	0.85	2.50

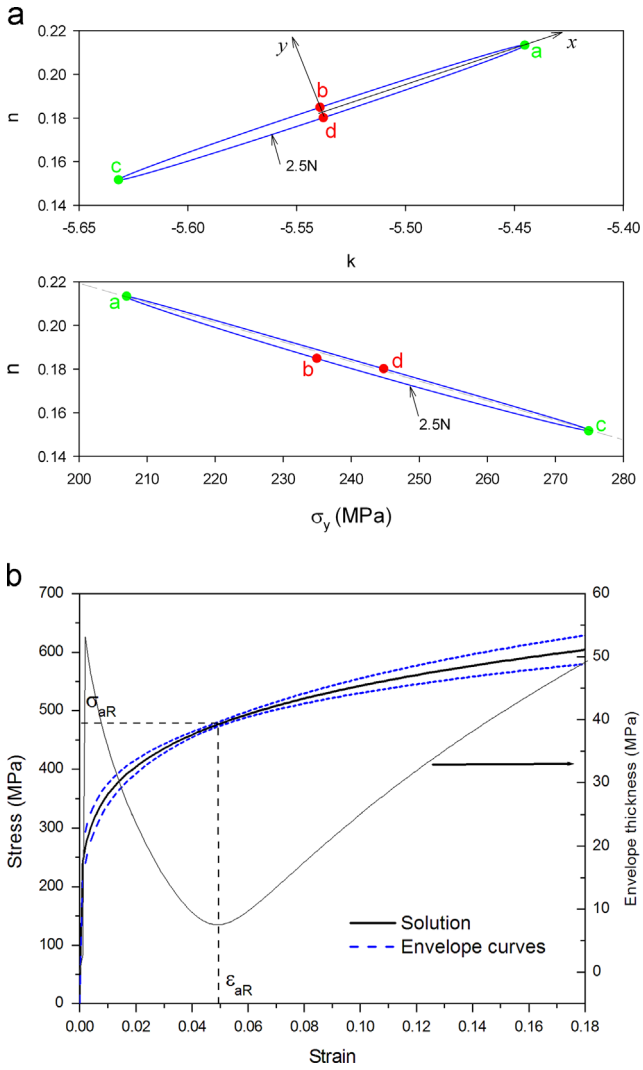

Fig. 7. (a) Ellipse corresponding to the maximal value of ERMS between the experimental curves (Table 1) [26]. (b) Identified solution and confidence domain limited with the envelope [26].

In this section, an identification method that allows identifying the Hollomon hardening law parameter set (σ_y, n) and the average representative strain was proposed for one specific penetration depth (h_{max}/R=0.2344 was used). As described above the average representative strain indicates the part of the Hollomon hardening law that is identified with the highest precision. In order to identify the hardening law of the material with the highest precision, the same

procedure is applied for multiple penetration depths in the following section.

4. Evaluation of the tensile properties from multiple h_{max}/R

4.1. Influence of penetration depth on the identified hardening law

As for the previous section, the average experimental indentation curve obtained for the 20MnB5 steel is used. Using the definition of the cone with the elliptical base (Eqs. (4) and (8)), the Hollomon hardening law parameter sets (σ_y, n) are calculated for various values of h_{max}/R ($0.0055 < h_{max}/R < 0.2344$). Fig. 8 shows that the maximum penetration depth has a strong influence on the values of the identified parameters of the studied material. Furthermore, a correlation between σ_y and n is observed. σ_y decreases and n increases when h_{max}/R increases. From these observations, it becomes difficult to make a choice of h_{max}/R to characterize a material with a Hollomon hardening law. A question is to be asked: which set of parameters should be considered as solution?

4.1.1. Discussion

The results presented in black color in Fig. 8 were obtained for the 20MnB5 steel for which the hardening law does not correspond perfectly to a Hollomon law. We propose to study the influence of the penetration depth on the identified hardening law for a material with a Hollomon hardening law. The F–h curve was obtained from FE simulation for a material with $\sigma_y = 260$ MPa and $n = 0.16$. From this indentation curve and using the definition of the cone with the elliptical base (Eqs. (4) and (8)), the Hollomon hardening law parameter sets (σ_y, n) are calculated.

From Fig. 8, it can be observed that the values of the identified Hollomon hardening law parameters are almost identical for every value of h_{max}/R. The small variations of the values of σ_y and n observed in Fig. 8 are only due to the precision of the minimization process in the proposed method (Eq. (8)). Hence, when the hardening law of the material corresponds perfectly to a Hollomon law, there is no influence of the penetration depth on the identified parameter set (σ_y, n). On the other hand, when the hardening law of the material does not correspond perfectly to a Hollomon law, the identified parameter set (σ_y, n) depends on the penetration depth (Fig. 8). From this result the problem of the uniqueness of solution in spherical indentation should be investigated.

Methods for the identification of the Hollomon parameter set (σ_y, n) from spherical indentation curve, F–h, were proposed in many studies [11,12,16–18,20–22]. In each study, one value of maximum penetration depth was chosen and was considered as sufficient to characterize the studied materials. No clear explanation on the choice of this value was given. For example, Lee et al. [16] proposed a model for the identification of the Hollomon hardening law parameter sets (σ_y, n). They chose a maximal ratio $h_{max}/R = 0.12$ with no justification. Later, in 2010, Lee et al. [17] showed that there could be a problem of uniqueness of solution for $h_{max}/R = 0.12$. They showed that two dissimilar materials may produce quite similar F–h curves for shallow indentation, i.e. $h_{max}/R = 0.12$. They also showed that as indentation depth increases, the F–h curves clearly separate from each other. This features inspired the authors [17] to develop a modified method for a deeper spherical indentation test, i.e. $h_{max}/R = 0.4$. The reason why this choice would definitely solve the problem of uniqueness of the solution was not given.

We show that the value of the identified parameter set (σ_y, n) is about the same independently of the value of h_{max}/R in the case of a material with a hardening law which corresponds perfectly to a Hollomon law (Fig. 8). In the case of a material with a hardening law which does not correspond to a Hollomon law, Fig. 8 shows that the values of the identified parameter set (σ_y, n) depend on the value of h_{max}/R. In the following part, a procedure of characterization which takes into account the values of the identified parameter sets (σ_y, n) obtained for all values of h_{max}/R is proposed.

4.2. Identification using the average representative strain

In Section 3 the average representative strain was only used to give additional information on the part of the hardening law that is identified with the highest precision. In this section the average representative strain is used to build the hardening law of the material point by point.

Using Eqs. (4), (7) and (8), a material parameter set (σ_y, n) and an average representative strain ε_{ar} are determined for each value of h_{max}/R. Using the fact that the higher the h_{max}/R ratio the higher ε_{ar} is, various sets (ε_{ar}, σ_{ar}) are determined for various h_{max}/R. This way, the hardening law of the material is built up with different sets (ε_{ar}, σ_{ar}). Fig. 9 shows that the built-up hardening law is very close to the tensile test curves of the material.

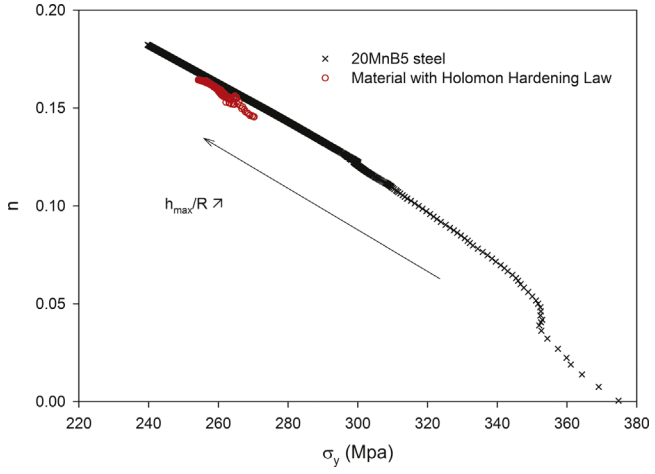

Fig. 8. Material parameter sets (σ_y, n) identified with spherical indentation for different penetration depths ($0.0055 < h_{max}/R < 0.2344$) for the case of 20MnB5 steel alloy (Section 2) and the case of a material with $\sigma_y = 260$ MPa and $n = 0.16$ (FE simulation result).

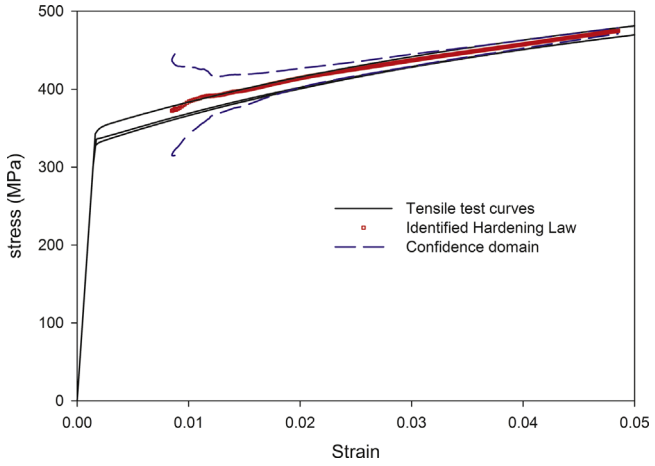

Fig. 9. Tensile test curves, hardening law identified with the proposed method and confidence domain determined with the proposed method.

4.2.1. Discussion

In Section 4.1 the question of uniqueness of solution was invoked for the case of 20MnB5 steel. We show in Fig. 8 that different Hollomon hardening law parameter sets (σ_y, n) are identified depending on the value of h_{max}/R. There is no reason to choose one specific material parameter set (σ_y, n) among the identified ones. The Hollomon hardening laws, obtained from parameter sets (σ_y, n) identified for small values of h_{max}/R, represent better the beginning of the plastic flow of the material. In a similar way, the Hollomon hardening laws, obtained from parameter sets (σ_y, n) identified for high values of h_{max}/R, represent better the plastic flow of the material for high values of strain. The procedure presented in this study allows considering all the identified Hollomon hardening laws obtained from small to large values of h_{max}/R. For each one of these laws, the corresponding point (ε_{ar} σ_{ar}) is considered because it is for this point that the result is the most precise when using the F–h curve for the identification of the hardening law. Using the built-up hardening law with the various sets (ε_{ar} σ_{ar}), no value of h_{max}/R ratio is considered more important than the others. With the proposed method, all h_{max}/R between 0.0055 and 0.2344 are equally considered and no unjustified choice was made on the value of the used h_{max}/R for the identification of the hardening law of the material. Even more, the range of plastic strains, for which the hardening is identified, is directly obtained, i.e. between 0.012 and 0.049 for the studied case. The proposed method is similar to the methods [10,13,15,19,27] based on the measure of applied load and contact radius from which the hardening law is built up point per point. The advantage of the proposed method is that the average representative strain is directly determined from measured parameters (F and h), which is not the case for the methods cited above. In these methods, the representative strain is obtained from the value of contact radius which is calculated from the value of penetration depth using models. In the studies on the representative strain in spherical and Vickers indentations, it was shown that the values of representative strain obtained from the F–h relationship are smaller than those obtained from the F–a relationship [28]. The use of the F–a relationship in addition to the F–h relationship must thus lead to the identification of complementary parts of the hardening law of a material.

4.3. Confidence domain

In order to take into account experimental imprecision and material heterogeneity, E_{RMS} is calculated between the average experimental curve and each one of the four experimental curves. The variation of this error as a function of h_{max}/R for the four experimental tests is presented in Fig. 10. From these errors, the maximal value of E_{RMS} is considered for each value of h_{max}/R. The average curve associated to the maximal value of E_{RMS} leads to the characterization of a confidence domain that takes into account the experimental imprecision and the material heterogeneity. Therefore, since one point of the hardening law is identified for each penetration depth, the confidence domain described in Section 2 is reduced to a minimum value and a maximum value of stress for each h_{max}/R. This way, the confidence domain is built up point by point.

For each ε_{aR}, the maximum and the minimum values of stress are determined using the material parameter sets (σ_y, n), corresponding to the points b and d of the isovalue ellipse represented in Fig. 7(a) as follow:

$$\begin{array}{ll} \text{point b} & \text{point d} \\ k = k_0 - Y\ \sin\ \theta_{AR} & k = k_0 + Y\ \sin\ \theta_{AR} \\ n = n_0 + Y\ \cos\ \theta_{AR} & n = n_0 - Y\ \cos\ \theta_{AR} \end{array} \quad (9)$$

The confidence domain built-up from the average experimental F–h curve is presented in Fig. 11. All the hardening laws that are located inside the confidence domain lead to F–h curves that give E_{RMS} smaller than the maximal value of E_{RMS} represented in Fig. 10. Thus the confidence domain regroups all possible solutions taking into account the experimental imprecision and the material heterogeneity. The four F–h curves, presented in Fig. 3, were used to characterize the material and the identified hardening laws are presented in Fig. 11. It can be observed in this figure that the four hardening laws are located inside the confidence domain.

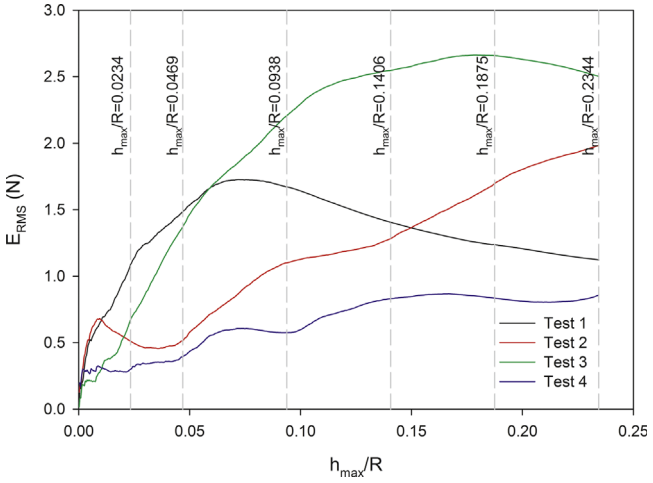

Fig. 10. Evolution of the error between the average curve and the four indentation curves as a function of the ratio penetration depth over indenter radius.

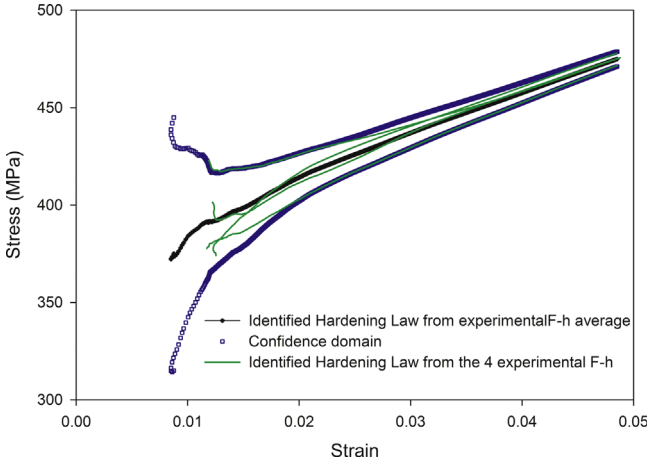

Fig. 11. Confidence domain and the four identified hardening laws determined from each one of the experimental F–h curves.

4.3.1. Discussion

Fig. 11 shows that the width of the confidence domain decreases with the increase in penetration depth. This result shows that the higher the penetration depth, the higher the precision of the identification from a F–h curve is. Six values of h_{max}/R are considered, see Fig. 12. For these six values of h_{max}/R, six values of E_{RMS} corresponding to the maximal experimental errors are obtained (see Fig. 10). Fig. 12 shows the six isovalues of E_{RMS} obtained in the diagram [σ_y, n]. It can be seen in this figure that the quasi-ellipses corresponding to the isovalues of E_{RMS} rotates with the variation in h_{max}/R value. The higher the value of h_{max}/R, the higher the values of θ_{ar} and ε_{ar} are.

The surface of each quasi-ellipse decreases when h_{max}/R increases (Fig. 12). This result confirms that because of the

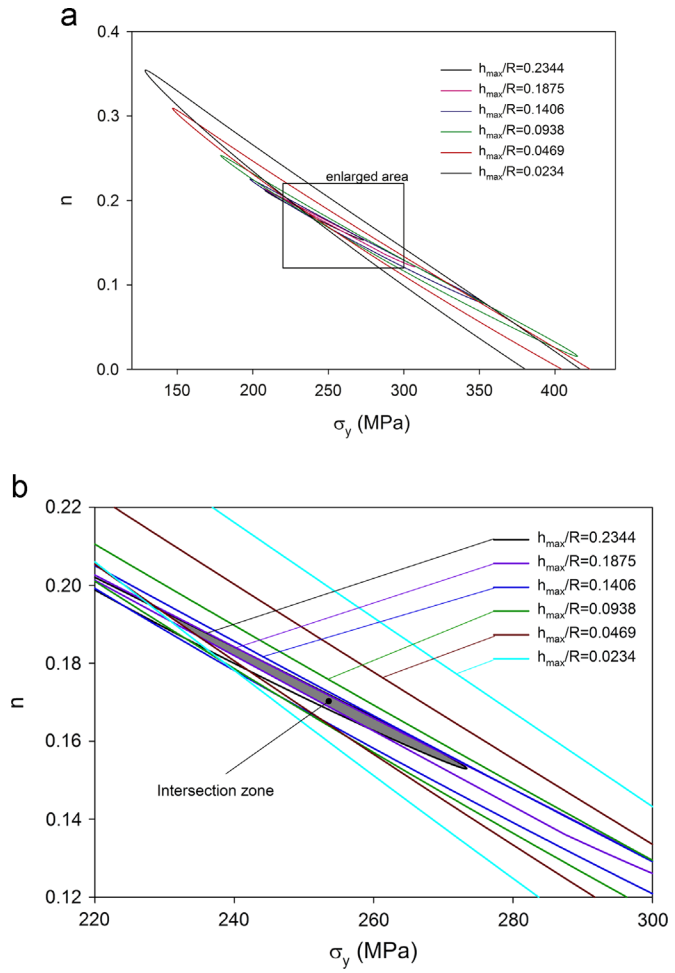

Fig. 12. Quasi-ellipses corresponding to the isovalues of the considered penetration depths: (a) total domain and (b) enlarged area around the intersection zone.

experimental imprecision, the smaller the penetration depth, the smaller the precision of the identified results is.

The surface corresponding to the intersection zone of the quasi-ellipses obtained for different values of h_{max}/R (Fig. 12(b)) should be considered for the identification of the Hollomon law of the material. For all these values of h_{max}/R, the material parameter sets located inside the intersection zone lead to F–h curves that give E_{RMS} smaller than the maximal value of the experimental error.

The results presented in Section 4 illustrate the problem of the uniqueness of the solution and the influence of the choice of penetration depth. The proposed method allows identifying the hardening law of the material for specific values of strain taking into account experimental imprecision and material heterogeneity.

The influence of the choice of the error (E_{RMS} in our case) is studied in the following section.

5. Influence of the choice of error

The procedure proposed above is applied to obtain the hardening law of the 20MnB5 steel using a different definition of error. This error is defined with the following equation:

$$RE_{RMS}(h_{max}/R) = 100\sqrt{\frac{1}{h_{max}}\int_0^{h_{max}}\left(\frac{F_1-F_2}{F_1}\right)^2 dh} \quad (10)$$

where RE_{RMS} is the root mean square relative error expressed in percentage.

E_{RMS} and RE_{RMS} do not depend on the number and on the distribution of the points of the experimental F–h curves respectively. Contrary to E_{RMS}, RE_{RMS} is defined so that the value of the error is equally influenced by small and high values of load. Since the proposed average representative strain is determined from the distribution of the error between an experimental curve and the F–h curves of the database, the error definition has an influence on the determined average representative strain (Fig. 13).

Moreover, the identified Hollomon hardening law parameter sets depend on the choice of the error. For example, for $h_{max}/R=0.2344$, the identified Hollomon hardening law parameter set, $\sigma_y=264$ MPa and $n=0.161$, obtained from RE_{RMS} is different from that calculated using E_{RMS}, i.e. $\sigma_y=240$ MPa and $n=0.182$.

Using the sets $(\varepsilon_{ar}, \sigma_{ar})$ determined with RE_{RMS} for various h_{max}/R, the hardening law of the material is built up point by point (Fig. 14). Despite the differences observed between the identified Hollomon hardening law parameter sets (σ_y, n) obtained from RE_{RMS} and E_{RMS}, Fig. 14 shows that the built-up hardening law superimposes the tensile test curves. This result confirms that the average representative strain indicates perfectly the part of the hardening law that is identified when using a F–h indentation curve. With the proposed procedure, the error formula only

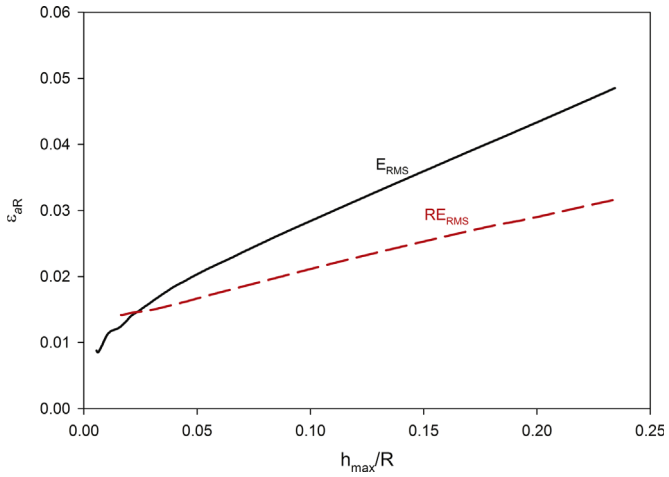

Fig. 13. Comparison between the variation of the average representative strains determined with E_{RMS} and RE_{RMS} as a function of h_{max}/R.

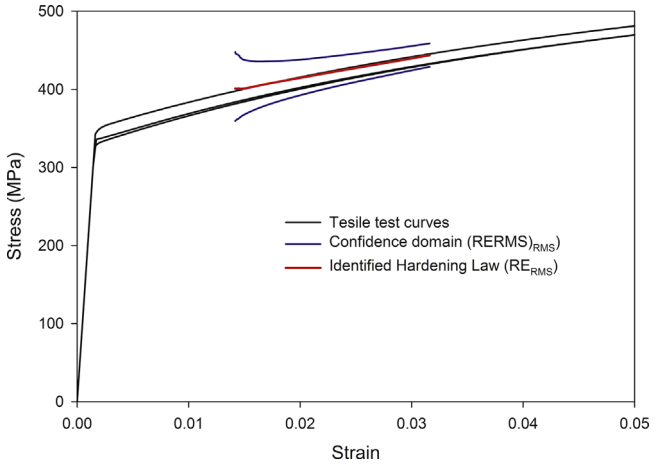

Fig. 14. Tensile test curves, hardening law identified with the proposed method using RE_{RMS} and confidence domain determined with the proposed method using RE_{RMS}.

influences the range of strain in which the hardening law is identified.

The comparison between Figs. 9 and 14 shows that the width of the confidence domain obtained with RE_{RMS} is higher than the one obtained with E_{RMS}. Hence, E_{RMS} leads to better precision than RE_{RMS}.

5.1. Discussion

As previously mentioned, the points of the experimental F–h curve do not have the same influence on the identified results when RE_{RMS} and E_{RMS} are used. The influence of the error formula on the values of the plastic properties of materials extracted from the spherical indentation loading curve was expected since h_{max}/R has an influence on these values. This influence was never studied in previous works [11,12,16–22]. Moreover, neither the error formula used to obtain the analytical expressions of the F–h curve as a function of material properties, nor the error formula used to evaluate the hardening law from this analytical expressions were given in these works. We show in this study that the influence of the error formula and the value of h_{max}/R should be considered when we use methods to evaluate the stress–strain curve from the F–h indentation curve.

6. Conclusion

In this study, a new method to extract the hardening law of materials from an instrumented spherical indentation loading curve is proposed. The results obtained with this method are very satisfactory when compared to the tensile test curves. Using the proposed average representative strain, this method takes into account multiple difficulties that were not specified in the literature:

- Depending on the value of the penetration depth, various Hollomon hardening law parameter sets (σ_y, n) can be identified from a single F–h spherical indentation curve. The proposed method allows considering all these parameter sets. Each penetration depth is considered to identify one point of the hardening law.
- The extraction of a stress–strain curve of a material from an indentation test only gives precise result for a range of strain. This range of strain is obtained with the proposed method.
- It is impossible to obtain two or more perfectly similar experimental indentation curves. Using the average experimental curve and the maximal experimental error, the proposed method allows identifying a confidence domain which takes into account the experimental imprecision and the material heterogeneity.
- Different Hollomon hardening law parameter sets (σ_y, n) are obtained when different error formula are used to calculate the gap between indentation curves. With the proposed procedure, the identified stress–strain curve does not depend on the error formula. The choice of the error only influences the range of strain in which the hardening law is identified and the width of the confidence domain.

References

[1] R.R. Ambriz, D. Chicot, N. Benseddiq, G. Mesmacque, S.D. de la Torre, Eur. J. Mech. A Solids 30 (2011) 307.
[2] N.A. Branch, N.K. Arakere, G. Subhash, M.A. Klecka, Int. J. Plast. 27 (2011) 728.
[3] K.-H. Chung, W. Lee, J.H. Kim, C. Kim, S.H. Park, D. Kwon, K. Chung, Int. J. Solids Struct. 46 (2009) 344.
[4] G. Das, M. Das, S. Sinha, K.K. Gupta, S. Chakrabarty, A.K. Ray, Mater. Sci. Eng. A 513–514 (2009) 389.
[5] L.M. Farrissey, P.E. McHugh, Meas. Interpret. Intern./ Residual Stress 399 (2005) 254.
[6] C. Moussa, O. Bartier, G. Mauvoisin, P. Pilvin, G. Delattre, J. Mater. Res. 27 (2012) 20.
[7] A. Nayebi, R. El Abdi, O. Bartier, G. Mauvoisin, M. Buisson, J. Mater. Process. Technol. 141 (2003) 276.
[8] K. Tunvisut, E.P. Busso, N.P. O'dowd, H.P. Brantner, Philos. Mag. A 82 (2002) 2013.
[9] M. Zhao, Y. Xiang, J. Xu, N. Ogasawara, N. Chiba, X. Chen, Thin Solid Films 516 (2008) 7571.
[10] J.-H. Ahn, D. Kwon, J. Mater. Res. 16 (2001) 3170.
[11] Y. Cao, X. Qian, N. Huber, Mater. Sci. Eng. A 454–455 (2007) 1.
[12] Y.P. Cao, J. Lu, Acta Mater. 52 (2004) 4023.
[13] J.S. Field, M.V. Swain, J. Mater. Res. 10 (1995) 101.
[14] E. Jeon, J.-Y. Kim, M.-K. Baik, S.-H. Kim, J.-S. Park, D. Kwon, Mater. Sci. Eng. A 419 (2006) 196.
[15] J.-Y. Kim, K.-W. Lee, J.-S. Lee, D. Kwon, Proceedings of the 33rd International Conference on Metallurgical Coatings and Thin Films, ICMCTF'06, vol. 201, 2006, p. 4278.
[16] H. Lee, J. Haeng Lee, G.M. Pharr, J. Mech. Phys. Solids 53 (2005) 2037.
[17] J.H. Lee, T. Kim, H. Lee, Int. J. Solids Struct. 47 (2010) 647.
[18] N. Ogasawara, N. Chiba, X. Chen, Mech. Mater. 41 (2009) 1025.
[19] B. Taljat, T. Zacharia, F. Kosel, Int. J. Solids Struct. 35 (1998) 4411.
[20] M. Zhao, N. Ogasawara, N. Chiba, X. Chen, Acta Mater. 54 (2006) 23.
[21] N. Ogasawara, N. Chiba, X. Chen, J. Mater. Res. (2005) 2225.
[22] X. Chen, N. Ogasawara, M. Zhao, N. Chiba, J. Mech. Phys. Solids 55 (2007) 1618.
[23] H. Lan, T.A. Venkatesh, Philos. Mag. 87 (2007) 4671.
[24] Y.-T. Cheng, C.-M. Cheng, Mater. Sci. Eng. R Rep. 44 (2004) 91.
[25] H. Lan, T.A. Venkatesh, J. Mater. Res. 22 (2007) 1043.
[26] C. Moussa, X. Hernot, O. Bartier, G. Delattre, G. Mauvoisin, J. Mater. Sci. 49 (2014) 592.
[27] Y.-C. Kim, S.-K. Kang, J.-Y. Kim, D. Kwon, J. Mater. Sci. 48 (2013) 232.
[28] O. Bartier, X. Hernot, G. Mauvoisin, C. Moussa, Matér. Tech. 101 (2013).